Journal of the Chinese Society of Mechanical Engineers, Vol.46, No.6, pp633~641 (2025)

Heat Transfer Mechanism Analysis of Metal Hydride Hydrogen Storage Reactor Based on Meyer Wavelet Finite Element Model

Yuebing Li*, Bin Zhao**, Diankkui Gao***, Lizhi Xu****and Yuanyuan Zhang*****

Keywords: Meyer wavelet finite element model, Heat transfer mechanism, metal hydride hydrogen storage reactor.

ABSTRACT

To reveal heat transfer mechanism of metal hydride hydrogen storage reactor (MHHSR) efficiently and accurately. Meyer wavelet finite element model (MWFEM) is built integrating MWSF to conventional finite element model, which can effectively implement heat transfer analysis of MHHSR. Firstly, heat transfer models of MHHSR is established, which contains governing equations of metal hydride bed, governing equations of heat exchange fluid, and corresponding heat transfer boundary conditions. Secondly, MWSF is considered as interpolation function to build MWFEM. Finally, MgH_2 reactor is selected as object to conduct heat transfer analysis, effect of hydrogen supply pressure, heat exchange fluid temperature, heat exchange fluid velocity and porosity on heat transfer law of MgH2 reactor are achieved by proposed MWFEM, conventional finite element model, B-spline wavelet finite element model, Daubechies wavelet finite element model and experiment. Heat transfer mechanism of MgH_2 reactor is acquired, results offer significant basis for optimal design of MgH_2 reactor, accuracy and efficient of proposed MWFEM are validated.

Paper Received June, 2024. Revised September, 2024. Accepted January, 2025. Author for Correspondence: Bin Zhao.

* *Graduate Student, School of Mechanical Engineering, Liaoning Petrochemical University, Fushun, China 113001.*

** *Professor, School of Mechanical Engineering, Liaoning Petrochemical University, Fushun, China 113001.*

*** *Experimenter, School of Mechanical Engineering, Liaoning Petrochemical University, Fushun, China 113001.*

**** *Associate Professor, School of Mechanical Engineering, Liaoning Petrochemical University, Fushun, China 113001.*

***** *Lecturer, School of Mechanical Engineering, Liaoning Petrochemical University, Fushun, China 113001.*

INTRODUCTION

Hydrogen belongs to a new clean energy, which is in an critical role of future energy system. Hydrogen energy has big ignite and can be accessed conveniently. Generally, Hydrogen can be stored as gas, liquid and solid, which fits various working environments. Hydrogen can be applied in fuel cell and nuclear fission fusion. Hence, it is necessary to enhance hydrogen utilizing quality. Hydrogen storage is an important problem of using hydrogen energy, it is significant to conduct hydrogen storage research. Hydrogen storage generally concludes high pressure gas storage, low temperature liquid storage, physical adsorption storage, organic liquid storage, coordination compound storage, and metal hydride storage. High pressure gaseous storage is simple, but it has shortcomings such as low storage efficiency, high storage capacity, high cost, worse security, and multiple energy expend. Low temperature liquid storage has shortcomings of multiple energy expend and big fluctuation. Physical adsorption storage is disturbed by environment significantly. Organic liquid storage expends excess heat and cost, it is three phase mixed storage method, which requires more complicated reactor. Coordination compound storage is efficient, but it has bad reversible hydrogen absorption capability, therefore it is difficult to achieve application. Metal hydride storage has advantages of big storing density, mild using environment, perfect cycle performance, so it is a effective hydrogen storage means. Hydrogen absorption process of metal hydride is a reversible reaction with strong thermal effect and mass transfer, it is important to conduct heat transfer analysis of MHHSR.

So far, heat transfer analysis of MHHSR has been concerned by some scholars. Atef et al.(2022) analyzed heat and mass transfer law of a metal hydride reactor, and put forward thermal supplier measurements. Rahul and Sharad (2021) revealed heat transfer rules of metal hydrogen reactor based on ANSYS, and effect of nanofluid on heat transfer rate of reactor is gained. Maxim D. Nashchekin et al. (2020) analyzed heat transfer enhancing laws of a metal hydrogen reactor . Tao and Xu (2022) revealed

heat transfer rules of a MHHSR, and put forward optimal design means of reactor [4]. Sayantan and Muthukumar (2023) conducted heat transfer experiment of MHHSR. According to available research achievements, heat transfer analysis has played critical role in enhancing performance of MHHSR.

Hear transfer process of MHHSR belongs to a typical nonlinear problem, a proper method should be chosen to enhance analysis precision and efficiency. Wavelet finite element method (WFEM) is developed by combining traditional finite element method and wavelet transform. Based on multiple resolution ability of wavelet transform, analysis precision and efficiency of wavelet finite element model can be improved without refining mesh. Zuo et al. (2022) developed a B-spline WFEM that was applied to analyze thermo-mechanical coupling mechanism of composite plate. Joglekar (2020) developed a WFEM that could analyze nonlinear frequency mixing in Timoshenko beam with breathing crack accurately. Miguel et al. (2022) deveoped a WFEM that analyzed electromagnetic device performance efficiently. As seen from existing achievements, WFEM has significant superiority in dealing with nonlinear problem. To further enhance analysis effectiveness, Meyer wavelet is chosen to establish MWFEM because it has many merits, such as quick attenuation velocity, and narrow spectrum. Meyer wavelet has been applied in many fields. Zulqurnain et al. (2021) developed a fractional Meyer wavelet neural network model, which has better performance according to comparative analysis results. Wu (2019) developed Meyer wavelet transform with edge angle tracking capability for image edge procession. So this research aims to establish MWFEM that is applied to heat transfer analysis of MHHSR, which can improve analysis precision and efficiency.

HEAT TRANSFER MODEL OF MHHSR

Heat transfer between heat exchange fluid and bed in MHHSR is complex, to simplify computational model, following hypotheses are suggested:

Hypothesis 1: Heat properties of metal hydride and hydrogen are stable.

Hypothesis 2: Local heat balance in metal hydride reaction bed is effective.

Hypothesis 3: Upper and lower end surfaces of hydrogen tube and reactor are insulated.

Hypothesis 4: Fluid is incompressible.

Governing equations of metal hydride bed

Mass conservation equation of hydrogen is formulated by (Shafiee and McCay, 2016)

$$\tau\frac{\partial\rho_{H_2}}{\partial t}+\nabla\cdot(\rho_{H_2}\vec{u}_{H_2})=-\dot{M} \tag{1}$$

where τ represents porosity, ρ_{H_2} represents density of hydrogen, $\vec{u}_{H_2}$ represents velocity of hydrogen, $\dot{M}$ represents hydrogen mass absorbed or released.

Mass conservation equation of metal hydride bed layer is formulated by

$$\dot{M}=\frac{\partial\rho_{bl}}{\partial t}(1-\tau) \tag{2}$$

where ρ_{bl} represents density of metal hydride.

Energy conservation equation is formulated by

$$(\rho C_p)_e\frac{\partial T}{\partial t}+\rho_{H_2}C_{p,H_2}\vec{u}_{H_2}\nabla T=\nabla\cdot(\lambda_e\nabla T)+\dot{M}\frac{\Delta H}{M_{H_2}} \tag{3}$$

where $(\rho C_p)_e$ represents effective volumetric heat capacity, T represents temperature, C_{p,H_2} represents specific heat capacity of hydrogen, λ_e represents effective thermal conductivity, ΔH represents enthalpy, M_{H_2} represents molecular weight of hydrogen.

Where effective volumetric heat capacity is calculated by

$$(\rho C_p)_e=\tau\rho_{H_2}C_{p,H_2}+(1-\tau)\rho_{bl}C_{p,bl} \tag{4}$$

Effective thermal conductivity is calculated by

$$\lambda_e=\tau\lambda_{H_2}+(1-\tau)\lambda_{bl} \tag{5}$$

where λ_{H_2} represents thermal conductivity of hydrogen, λ_{bl} represents thermal conductivity of metal hydrogen bed layer.

Hydrogen absorption equilibrium pressure is computed by (Bai et al., 2022)

$$P_{E,a}=\sum_{i=1}^{n}\phi_i\cdot\gamma_{hm}^{i}\cdot e^{\frac{\Delta H}{R}(\frac{1}{T}-\frac{1}{303})} \tag{6}$$

where ϕ_i represents hydrogen absorption equilibrium pressure polynomial parameter, γ_{hm} represents ratio of hydrogen to metal atom, R represents standard gas constant.

Hydrogen desorption equilibrium pressure is computed by (Jiang et al., 2023)

$$P_{E,a}=\sum_{i=1}^{9}\phi_i\cdot\gamma^{i}\cdot e^{\frac{\Delta H}{R}(\frac{1}{T}-\frac{1}{303})} \tag{7}$$

Governing equation of heat exchange fluid

Continuity equation of heat exchange fluid flow is formulated by (Malleswararao et al., 2022)

$$\nabla\vec{u}_f=0 \tag{8}$$

where $\vec{u}_f$ represents velocity of heat exchange

fluid.

Energy conservation equation of heat exchange fluid is formulated by (Saucedo et al., 2022)

$$(\rho C_p)_f \frac{\partial T_f}{\partial t} + (\rho C_p)_f \vec{u}_f \nabla T_f = \nabla \cdot (\lambda_f \nabla T_f) \quad (9)$$

where $(\rho C_p)_f$ is volumetric heat capacity of heat exchange fluid, T_f represents temperature of heat exchange fluid, λ_f represents thermal conductivity of heat exchange fluid.

When Re is less than 2300, heat exchange fluid flow is described based on Navier-Stokes equation:

$$\rho_f \vec{u}_f \nabla \vec{u}_f = \nabla \cdot [\mu_f (\nabla \vec{u}_f + (\nabla \vec{u}_f)^T) - \nabla P_f) \quad (10)$$

where ρ_f represents density of heat exchange fluid, μ_f represents temperature viscosity of heat exchange fluid, P_f represents pressure of heat exchange fluid.

When Re is larger than 10000, heat exchange fluid flow is described based on $k-\varepsilon$ model :

$$\rho_f \vec{u}_f \nabla \vec{u}_f = \nabla \cdot [(\mu_f + \mu_T)(\nabla \vec{u}_f + (\nabla \vec{u}_f)^T] - \nabla P_f \quad (11)$$

where μ_T is turbulence viscosity.

Turbulence kinetic energy equation is formulated by

$$\rho_f \vec{u}_f \nabla k = \nabla \cdot [(\mu_f + \frac{\mu_T}{\sigma_k}) \nabla k] + \mu_T [\nabla u_f : (\nabla u_f + (\nabla u_f)^T)] - \rho_f \psi \quad (12)$$

where k represents turbulence kinetic energy, σ_k represents Prandtl constant, ψ is computed by

$$\psi = C_\mu \frac{3k^{3/2}}{4L_T} \quad (13)$$

where C_μ represents constant, L_T represents turbulence length.

Turbulent energy dissipation rate equation is formulated by

$$\rho_f \vec{u}_f \nabla \varphi = \nabla \cdot [(\mu_f + \frac{\mu_T}{\sigma_\varphi}) \nabla \varphi] + C_{\varphi 1} \frac{\varphi}{k} \mu_T [\nabla u_f : (\nabla u_f + (\nabla u_f)^T)] - C_{\varphi 2} \rho_f \frac{\varphi^2}{k} \quad (14)$$

where $C_{\varphi 1}$ and $C_{\varphi 2}$ represent constants, σ_φ represents Prandtl constant of turbulence energy dissipation rate.

Boundary condition

End surface of MHHSR insulating wall has no heat exchange, and boundary conditions are listed as follows (Aydin et al., 2022; Li et al., 2023)

$$\frac{\partial T_i}{\partial n} = 0, \quad i = s, w, f \quad (15)$$

where subscript "s" represents metal hydride, subscript "w" represents heat exchange pipe, subscript "f" represents heat exchange fluid.

$$\frac{\partial P_{H_2}}{\partial n} = 0, \quad (16)$$

$$\frac{\partial P_f}{\partial n} = 0, \quad (17)$$

Hydrogen inlet boundary conditions are as follows:

Hydrogen absorption stage:

$$P_{H_2} = P_a, \ \nabla T \cdot n = 0 \quad (18)$$

Hydrogen desorption stage:

$$P_{H_2} = P_d, \ \nabla T \cdot n = 0 \quad (19)$$

Boundary conditions of inner wall of MHHSR are as follows:

$$\lambda_f \frac{\partial T_f}{\partial n} = h_{f,i}(T_f - T_w) \quad (20)$$

$$\lambda_w \frac{\partial T_w}{\partial n} = h_{f,i}(T_w - T_f) \quad (21)$$

where $h_{f,i}$ represents convective heat transfer factor of heat exchange fluid inside heat exchange pipe.

Boundary conditions of outer wall of heat exchange pipe are as follows:

$$\lambda_s \frac{\partial T_s}{\partial n} = h_{f,e}(T_s - T_w) \quad (22)$$

$$\lambda_w \frac{\partial T_w}{\partial n} = h_{f,e}(T_w - T_s) \quad (23)$$

$$\lambda_w \frac{\partial T_s}{\partial n} = h_f(T_s - T_f) \quad (24)$$

where $h_{f,e}$ represents convective heat transfer coefficient of heat exchange fluid outside heat exchange pipe.

Inlet boundary conditions of heat exchange fluid are:

$$u_{f,x} = u_{f,y} = 0, \ u_{f,z} = u_{in}, \ T_f = T_{in} \quad (25)$$

Outlet boundary conditions of heat exchange fluid are (Lesmana and Aziz, 2023):

$$P_f = 0, \quad \nabla \cdot (\lambda_f \nabla T_f) = 0 \quad (26)$$

Outlet boundary condition of MHHSR is formulated by

$$\lambda_s \frac{\partial T_s}{\partial n} = h_a(T_s - T_e) \quad (27)$$

$$\lambda_a \frac{\partial T_e}{\partial n} = h_a(T_e - T_s) \quad (28)$$

where h_a represents convective heat transfer factor of air, T_e represents environmental temperature.

CONSTRUCTION OF MWFEM

Meyer wavelet scale function (MWSF) is formulated by (Zhang, 2022)

$$\tilde{\psi}=\begin{cases}1 & |\omega|\le\frac{2\pi}{3}\\ \cos(\frac{\pi}{2}\tilde{s}(\frac{3|\omega|}{2\pi}-1)) & \frac{2\pi}{3}<|\omega|\le\frac{4\pi}{3}\\ 0 & |\omega|\ge\frac{4\pi}{3}\end{cases} \quad (29)$$

It meets following conditions:

$\tilde{\psi}(2\omega)=H(\omega)\tilde{\psi}(\omega)$, $H(\omega)$ is 2π periodic function. $\sum_{k\in Z}|\tilde{\psi}(\omega+2k\pi)|^2\equiv 1$.

Where $\tilde{s}(x)$ represents fully smooth S-shaped function, which is formulated by

$$\tilde{s}=\frac{c(x)}{c(x)+c(1-x)} \quad (30)$$

where $g(x)$ represents continuous function on $(-\infty,\infty)$, when $x\le 0$, $c(x)=0$, and when $x>0$, $c(x)>0$, $c(x)$ is formulated by

$$c(x)=\begin{cases}Be^{-\frac{1}{x^n}} & x>0\\ 0 & x\le 0\end{cases} \quad (31)$$

where $B\neq 0$, $n\in N^+$, $n\in N^+$, $c(x)\in C^\infty(R)$.

MWSF is combined with conventional FEM to construct MWFEM through using it as interpolating function. 2D scale function on tensor product space is formulated by (Fu et al.,2021)

$$\phi=\phi_1\otimes\phi_2 \quad (32)$$

where $\otimes$ represents Kronecker signal, ϕ_1 and ϕ_2 are formulated by

$$\phi_1=[\tilde{\psi}_0^k(\xi),\tilde{\psi}_1^k(\xi),\cdots,\tilde{\psi}_{2^k+m-2}^k(\xi)] \quad (33)$$

$$\phi_2=[\tilde{\psi}_0^k(\gamma),\tilde{\psi}_1^k(\gamma),\cdots,\tilde{\psi}_{2^k+m-2}^k(\gamma)] \quad (34)$$

where $\tilde{\psi}_j^k(\gamma)$ represents 1D spatial MWSF at m order and k scale. ξ and γ are local coordination.

Temperature of MHHSR is formulated by

$$\theta(\xi,\gamma)=\vec{\phi}_1\otimes\vec{\phi}_2\cdot\vec{b}=\sum_{i,j}\tilde{\psi}_j^k(\xi)\tilde{\psi}_j^k(\gamma)\vec{b}_e \quad (35)$$

where $\vec{b}_e$ represents Meyer wavelet factor column vector, $\vec{b}_e=[\vec{b}_0,\vec{b}_1,\cdots,\vec{b}_{2^k+m-2}]$.

Thermal conductive equation of MHHSR is formulated by

$$\rho_{hsr}c_{hsr}\frac{\partial\theta}{\partial t}=k_{hsr}(\frac{\partial^2\theta}{\partial r^2}+\frac{1}{r}\frac{\partial\theta}{\partial r}+\frac{\partial^2\theta}{\partial z^2}) \quad (36)$$

where ρ_{hsr} represents density of MHHSR, c_{hsr} represents specific heat capacity of MHHSR, k_{hsr} represents thermal conductivity of MHHSR.

The variation equation of temperature field for equation (36) based on Ga1erkin method is derived, which is formulated by

$$\iint_e k_{hsr}\gamma(\frac{\partial Q_{ij}}{\partial\xi}\cdot\frac{\partial\theta}{\partial\xi}+\frac{\partial Q_{ij}}{\partial\gamma}\cdot\frac{\partial\theta}{\partial\gamma}+\rho_{hsr}c_{hsr}Q_{ij}\gamma\frac{\partial\theta}{\partial t})d\xi d\gamma-[\int_\Gamma k_{hsr}Q_{ij}\gamma\frac{\partial\theta}{\partial\vec{n}}dl=0 \quad (37)$$

where Q_{ij} represents weight function, which is calculated by

$$Q_{ij}=\tilde{\psi}_i(\xi)\tilde{\psi}_j(\gamma)=\Omega_{ij} \quad (38)$$

Following MEWFEM is obtained through substituting equations (35) and (38) into equation (37) (Joglekar, 2021).

$$\vec{H}^e\vec{b}^e+\vec{C}^e\vec{b}^e=\vec{L}^e \quad (39)$$

where $\vec{H}^e$ represents element heat capacity matrix, $\vec{C}^e$ represents element heat conduction matrix, $\vec{L}^e$ represents element load column vector.

$$\vec{H}^e_{i,j,l,k}=\int_0^1\int_0^1\rho_{hsr}c_{hsr}\Omega_{ij}\Omega_{lk}\gamma d\xi d\gamma \quad (40)$$

$$\vec{C}^e_{i,j,l,k}=\int_0^1\int_0^1 k_{hsr}\gamma(\frac{\partial\Omega_{ij}}{\partial\xi}\cdot\frac{\partial\Omega_{lk}}{\partial\xi}+\frac{\partial\Omega_{ij}}{\partial\gamma}\cdot\frac{\partial\Omega_{lk}}{\partial\gamma})d\xi d\gamma+\int_\Gamma h_a\Omega_{ij}\Omega_{lk}dl \quad (41)$$

Element heat capacity matrix, element heat conduction matrix, and element load column vector in physical space can be obtained through transforming element balance equation from Meyer wavelet coefficient space to physical space.

Temperature vector of Meyer wavelet finite element is represented by

$$\vec{\theta}^e=\vec{M}^e\vec{b}^e \quad (42)$$

where $\vec{M}^e=\vec{M}_1^e\otimes\vec{M}_2^e$, in which

$$\vec{M}_1^e=[\phi_1'(\xi_0),\phi_1'(\xi_1),\cdots,\phi_1'(\xi_{2^k+m-2})]' \quad (43)$$

$$\vec{M}_2^e=[\phi_2'(\gamma_0),\phi_2'(\gamma_1),\cdots,\phi_2'(\gamma_{2^k+m-2})]' \quad (44)$$

$$\vec{b}^e=(\vec{M}^e)^{-1}\vec{\theta}^e \quad (45)$$

Then, superposition of element matrix and treatment of boundary conditions are carried out, and total MWFEM with the element node temperature as unknown variable is obtained, which is formulated by

$$\vec{H}\vec{\theta}+\vec{C}\vec{\theta}=\vec{L} \quad (46)$$

HEAT TRANSFER MECHANISM ANALYSIS OF MHHSR

A cylindrical MgH_2 reactor is as research subject to conduct heat transfer analysis by MWFEM. Eight cylindrical thermal conductivity oil layers with same size are arranged in MgH_2 reactor, a circular

thermal conductivity oil layer with same material is arranged outside MgH_2 reactor, thermal conductivity oil is in a flowing status. Main material of MHHSR is magnesium powder, H_2 enters from middle of MHHSR. Diagram of MgH_2 reactor is as shown in figure 1.

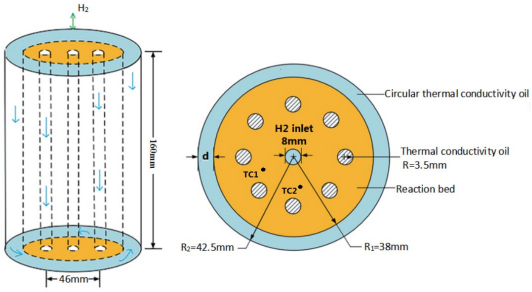

Fig.1 Diagram of MgH_2 reactor.

General chemical reaction equation for hydrogen desorption stage of MgH_2 is formulated by

$$MgH_2 \rightarrow Mg+H_2 \quad (47)$$

Performance parameters of Mg and H_2 are listed in Table 1.

Table 1. Main physical parameters of Mg and H_2

Parameter	Mg	H_2
Density/kg.m^{-3}	1740	0.0838
Molecular weight/kg.mol^{-1}	0.024	0.002
Thermal conductivity/W.m^{-1}K^{-1}	155.7	0.127
Specific heat capacity/J.kg^{-1}K^{-1}	102.5	14283
Saturated metal hydride density/kg.m^{-3}	1545	
Metal hydride particle diameter/ μ m	22.6	
Hydrogen absorption rate constant/s^{-1}	2.9×10^{8}	
Hydrogen absorption activation energy/J.mol^{-1}	124000	
Standard gas constant/J.K^{-1}.mol^{-1}		8.314
Reaction enthalpy/J.mol^{-1}		-75000
Porosity	0.31	

To check performance of proposed MWFEM, experimental results of MHHSR studied by Chaise et al. (2010) were used to test proposed model. To decrease error caused by mesh in numerical simulation, it is necessary to check mesh independence to cut down impact of mesh on analysis error. To thoroughly reflect reliability of MWFEM and scientificity of mesh partition, analysis result in hydrogen absorption stage at different meshes are applied to confirm its relative change rate χ that is computed by

$$\chi=\frac{|\theta_{bm}-\theta_{bn}|}{\theta_{bm}}\times 100\% \quad (48)$$

where θ_{bm} represents numerical simulation result with mesh m; θ_{bn} represents numerical simulation result with mesh n.

Number analysis of MgH_2 reactor bed temperature in hydrogen absorption stage under variouset mesh number is implemented, and mesh independent check curve is acquired that is illustrated figure 2. As seen from figure 2, when mesh number is over 59830, relative change rate of MgH_2 reactor bed temperature is less than 0.1%, and keeps a unchanged state, therefore optimal mesh number is taken as 59830 for balancing analysis precision and capability of computer.

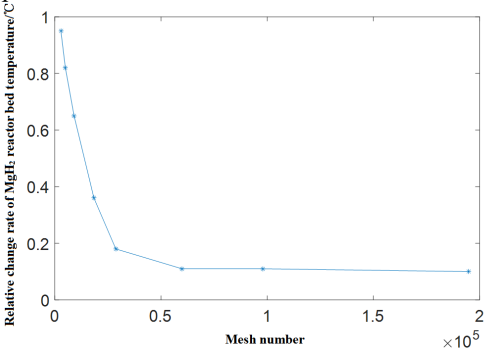

Fig.2 Mesh independent inspection curve of MgH_2 reactor bed temperature.

In addition, TFEM, B-spline wavelet finite element model (BSWFEM) and Daubechies wavelet finite element model (DWFEM) are also applied to conduct heat transfer analysis of same MHHSR. Mesh number of different models is listed in Table 2.

Table 2. Mesh number of different models.

Model	Number of elements
TFEM	130495
BSWFEM	66893
DWFEM	62034

Compared results of MgH_2 reactor bed temperature in absorption procession where initial and set-point conditions are 300℃ and 0.77MPa are listed in Table 3. Where TC1 and TC2 are testing points that are shown in Figure 1. As seen from Table 3, analysis error of TFEM ranges from 5.12% to 5.98%, analysis error of BSWFEM ranges from 2.69% to 3.69%, analysis error of DWFEM ranges from 2.20% to 3.01%, and analysis error of MWFEM ranges from 1.36% to 1.69%. Compared results illustrate that proposed MWFEM has higher precision than other models on MgH_2 reactor bed temperature. Analysis precision of TFEM is lowest among four models. Analysis precision of BSWFEM and DWFEM is relatively close, and is between that of MWFEM and TFEM.

Table 3. Compared results of MgH_2 reactor bed temperature in absorption procession.

Testing point	Time/min	Testing value/℃	TFEM		BSWFEM		DWFEM		MWFEM	
			Simulation result/℃	Error/%	Simulation result/℃	Error/%	Simulation result/℃	Error/%	Simulation result/℃	Error/%
TC1	10	331.4	348.8	5.25	342.7	3.41	339.5	2.44	336.9	1.66

	20	342.5	362.2	5.75	353.2	3.12	351.4	2.56	347.5	1.46
	30	355.3	373.5	5.12	366.7	3.21	364.6	2.62	360.3	1.41
	40	362.5	381.6	5.27	374.7	3.37	372.2	2.67	368.6	1.61
	50	364.6	383.8	5.27	375.3	2.93	373.6	2.47	369.9	1.5
	60	368.2	389.6	5.81	378.1	2.69	376.7	2.31	373.2	1.6
TC2	10	329.6	349.3	5.98	341.3	3.55	338.6	2.73	334.2	1.0
	20	340.6	360.1	5.73	352.4	3.46	349.2	2.52	345.5	1.4
	30	336.7	354.3	5.23	346.2	2.82	344.1	2.20	341.6	1.46
	40	331.5	350.4	5.70	343.2	3.53	340.5	2.71	336.2	1.42
	50	325.4	344.6	5.90	337.4	3.69	335.2	3.01	330.5	1.5
	60	319.8	338.4	5.81	331.3	3.60	329.3	2.97	324.6	1.50

Computation time of different models is listed in Table 4. As seen from Table 4, computation time of WMFEM is less than that of other models, therefore proposed WMFEM has higher computation efficiency than other models.

Table 4. Computation time of different models

Model	Computation time/s	
	TC1	TC2
TFEM	178.43	183.25
BSWFEM	88.62	89.06
DWFEM	86.53	87.94
WMFEM	46.78	47.32

Hydrogen supply pressure, heat exchange fluid temperature and heat exchange fluid velocity are main parameters of MgH2 reactor. Temperature of MgH2 reactor bed with different different operation parameters is obtained based on different models respectively.

Maximum temperature of MgH_2 reactor bed is calculated with different hydrogen absorption pressures based on different models, and analysis results are illustrated in Figure 3. As seen from Figure 3, maximum temperature of MgH2 reactor bed is proportional to hydrogen absorption pressure, when the pressure increases from 0.4MPa to 1.6MPa, MgH2 reactor bed maximum temperature increases from 591 K to 631 K, and average basic temperature of MgH2 reactor bed body increases by 40 K. The reason for this phenomena is that the higher the pressure, the better the reaction proceeds, and the better the reaction, the more heat will be released, resulting in an increase in temperature. Moreover MWFEM solution is closer to testing value than TFEM and DWFEM, better precision of MWFEM is also validated.

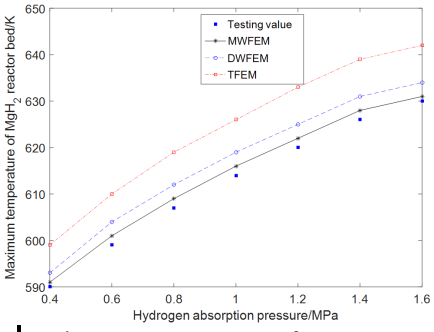

Fig. 3. Maximum temperature of MgH_2 reactor bed with different hydrogen absorption pressure.

Maximum temperature of MgH_2 reactor bed is calculated with various hydrogen heat exchange fluid temperatures based on different models, and analysis results are illustrated in Figure 4. As seen from Figure 4, when heat exchange fluid temperature rises from 293K to 333k, maximum temperature of MgH_2 reactor bed increases from 590K to 630K. Strong exothermic effect exists in hydrogen absorption process, when heat exchange fluid temperature is low, it can quickly exchange heat with MgH_2 reactor inside. Furthermore, MWFEM also acquires higher precision than other model.

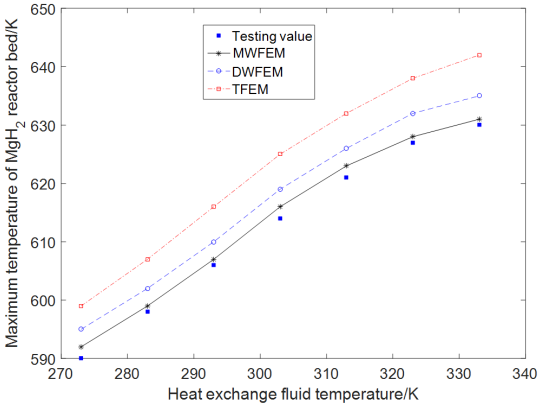

Fig. 4. Maximum temperature of MgH2 reactor bed with different heat exchange fluid temperature.

Heat exchange fluid velocity can affect turbulence characteristics of fluid, and affect heat transfer process of MgH_2 reactor bed. Maximum temperature of MgH_2 reactor bed with different heat exchange fluid velocity is obtained based on different models, which is shown in Figure 5. As seen from Figure 5, maximum temperature of MgH_2 reactor bed increases with increase of heat exchange fluid velocity. When heat exchange fluid velocity is less than 1m/s, increasing rate of maximum temperature of MgH_2 reactor bed is big. When heat exchange

fluid velocity is larger than 1m/s, increasing rate of maximum temperature of MgH_2 reactor bed is low. The main reason is that when heat exchange fluid velocity is larger than 1m/s, heat exchange fluid is in a completely turbulent status, and at this time, heat exchange fluid can quickly remove the reaction zone from the reactor. If heat exchange fluid velocity increases continuously, although it can enhance turbulence degree of heat exchange fluid, heat exchange fluid velocity control steps of heat transfer performance at this time are heat transfer rate near the heat exchange tube and rate at which heat is transferred to heat exchange fluid through wall of heat exchange tube, at this time, exchange fluid velocity has little effect on overall heat transfer performance of MgH_2 reactor.

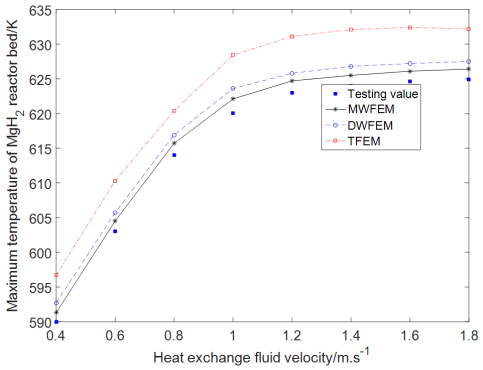

Fig. 5. Maximum temperature of MgH_2 reactor bed with different heat exchange fluid velocity.

Porosity is an important parameter for MgH_2 reactor, effect of porosity on heat transfer performance of MgH_2 reactor is analyzed based on different models, and analysis results are shown in Figure 6.

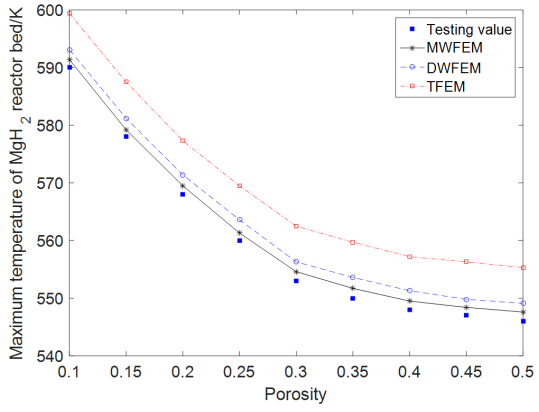

Fig. 6. Maximum temperature of MgH_2 reactor bed with different porosity.

As seen from Figure 6, maximum temperature of MgH_2 reactor bed decreases with increase of porosity, main reason for this phenomenon is that the larger the porosity is, the easier it is for heat to diffuse, therefore increasing porosity properly can effectively enhance heat transfer capability of MgH_2 reactor. When porosity is low, change rate of maximum temperature of MgH2 reactor is large. The main reason for this phenomenon is that MgH_2 powder has a good continuity when porosity is small.

CONCLUSIONS

Metal hydride hydrogen storage is a reversible reaction with strong heat transfer, to overcome high analysis cost and big dissipation error of TFEM on heat transfer analysis of MHHSR, MWFEM is deduced through combing MWSF and TFEM. MgH_2 reactor is used as research object to carry out heat transfer analysis based on MWFEM, TFEM, B-spline wavelet finite element model, Daubechies wavelet finite element model and experiment. Optimal mesh number of Meyer wavelet finite elements is taken as 59830 based on mesh independent analysis. Compared results of MgH_2 reactor bed temperature in absorption procession show that proposed MWFEM has higher analysis precision than other models on MgH_2 reactor bed temperature in absorption procession, and proposed WMFEM has higher efficiency than other models. Effect rules of Hydrogen supply pressure, heat exchange fluid temperature and heat exchange fluid velocity on heat transfer of MgH_2 reactor are acquired. When pressure increases from 0.4MPa to 1.6MPa, MgH_2 reactor bed maximum temperature increases from 591 K to 631 K. When heat exchange fluid temperature rises from 293K to 333k, maximum temperature of MgH_2 reactor bed increases from 590K to 630K. heat exchange fluid temperature rises from 293K to 333k, maximum temperature of MgH_2 reactor bed increases from 590K to 630K. Moreover, effect law of porosity on heat transfer of MgH2 reactor is also acquired, results illustrate that maximum temperature of MgH_2 reactor bed decreases with increase of porosity, when porosity is low, change rate of maximum temperature of MgH_2 reactor is large. Analysis results show that proposed MWFEM is a better means for heat transfer analysis of MHHSR, analysis results can offer theoretical basis for optimal design of MHHSR. The influence of the heat transfer of the column material characteristics should be analyzed in depth future.

REFERENCES

Atef, C., Slimane, M., Noureddine, G., Issam, F., Yacine, B., “Numerical investigation of heat and mass transfer during hydrogen desorption in a large-scale metal hydride reactor coupled to a phase change material with nano-oxide additives,” *Int. J. Hydrogen Energ.* Vol.47, No.32, 14611-14627 (2022).

Aydin, E.S., Yucel, O., “Computational fluid dynamics study of hydrogen production using concentrated solar radiation as a heat source,”

Energ. Convers. Manage. Vol. 276, No.116552 (2022).

Bai, X.S., Yang, W.W., Tang, X.Y., Dai, Z.Q., Yang, F.S., "Parametric optimization of coupled fin-metal foam metal hydride bed towards enhanced hydrogen absorption performance of metal hydride hydrogen storage device," *Energ.* Vol.243, No.123044 (2022).

Chaise, A., Rangop D., Martyp P., "Experimental and numerical study of a magnesium hydride tank," *Int. J. Hydrogen Energ.* Vol.35, No.12, pp.6311-6322 (2010).

Fu, S.B., Li, G.L., Craster, R., Guenneau, S., "Wavelet-based Edge Multiscale Finite Element Method for Helmholtz Problems in Perforated Domains," *Multiscale Model. Sim.* Vol.19, No.4, pp.1684-1709 (2021).

Jiang, B., Wang, H.N., Yu, K.W., Ma, J., Wang, S.M., Gao, Y.M., Li, L., "Zhang Xinwei, Cui Huiru, Tang Dawei, A high-efficient anisotropic continuum model for the optimization of heat transfer and chemical reaction in a packed-bed water gas shift reactor," *Fuel* Vol.333, No.2, pp.126493 (2023).

Joglekar, D.M., "Analysis of nonlinear frequency mixing in Timoshenko beams with a breathing crack using wavelet spectral finite element method," *J. Sound Vib.* Vol.488, No.115532 (2020).

Lesmana, L.A., Aziz, M., "Adoption of triply periodic minimal surface structure for effective metal hydride-based hydrogen storage," *Energ.* Vol.262, No.125399(2023).

Li, J., Zhang, Z.Q., Fu, Y., Chen, S.J., Xu, Y., Fan, H.X., "Numerical Simulation of Hydrogen Storage Process in MIL - 101(Cr) with Different Thermal Conductivity," *J. Petrochem. Univ.* Vol.36, No.3, pp.31-36 (2023).

Malleswararao, K., Aswin, N., Kumar, P., Dutta, P., Murthy, S.S., "Experiments on a novel metal hydride cartridge for hydrogen storage and low temperature thermal storage," *Int. J. Hydrogen Energ.* Vol.47, No.36, pp.16144-16155 (2022).

Maxim, D.N., Maria, V.M., Svetlana, B.M., Konstantin, B.M., "Enhancement of heat- and mass-transfer processes in a metal-hydride flow-through hydrogen-purification reactor," *Int. J. Hydrogen Energ.* Vol.45, No.46, pp.25013-25029 (2020).

Miguel, G.F., Patrick, K.P., Marcelo, G.V., "Electromagnetic device modeling using a new adaptive WFEM," *Math. Comput. Simulat.* Vol.172, pp.111-133 (2022).

Rahul U.U., Sharad, D.P., "Enhancement of heat and mass transfer characteristics of metal hydride reactor for hydrogen storage using various nanofluids," *Int. J. Hydrogen Energ.* Vol.46, No.37, pp. 19486-19497 (2021).

Saucedo, M.E.N., Arancibia-Bulnes, C.A., "Macias Juan Daniel, Ramirez-Cabrera Manuel Alejandro, Valades-Pelayo Patricio J., Heat transfer and chemical kinetics analysis of a novel solar reactor for hydrothermal processing," *Sol. Energ.* Vol.241, pp.372-385 (2022).

Sayantan, J., Muthukumar, P., "Design, development and hydrogen storage performance testing of a tube bundle metal hydride reactor," *J. Energ. Storage*, Vol.63, No.106936 (2023).

Shafiee, S., McCay, M.H., "Different reactor and heat exchanger configurations for metal hydride hydrogen storage systems - A review," *Int. J. Hydrogen Energ.* Vol.41, No.22, pp.9462-9470 (2016).

Tao, S., Xu, H.J., "Integration of hydrogen storage and heat storage in thermochemical reactors enhanced with optimized topological structures: Charging process," *Appl. Energ.* Vol.327, No.120138 (2022).

Wu, M.T., "Wavelet transform based on Meyer algorithm for image edge and blocking artifact reduction," *Inform. Sciences*, Vol.474, pp.125-135 (2019).

Zhang, Z.H., "Non-Separable Meyer-like Wavelet Frames," *Math.* Vol.10, No.13, pp.2296 (2022).

Zulqurnain, S., Muhammad, A.Z.R., Juan, L.G.G., Tareq, S., "Meyer wavelet neural networks to solve a novel design of fractional order pantograph Lane-Emden differential model," *Chaos Soliton. Fract.* Vol.152, No.111404 (2021).

Zuo, H., Chen, Y.X., Feng, J., "Thermo-mechanical coupling analysis of laminated composite plates using WFEM," *Thin Wall. Struct.* Vol.172, No.108911 (2022).

NOMENCLATURE

c_{hsr} specific heat capacity of MHHSR

C_{p,H_2} represents specific heat capacity of hydrogen

$C_{\varphi 1}$ and $C_{\varphi 2}$ constants

$\vec{C}^e$ element heat conduction matrix

h_a convective heat transfer factor of air

$h_{f,i}$ convective heat transfer factor of heat exchange fluid inside heat exchange pipe

$h_{f,e}$ convective heat transfer coefficient of heat exchange fluid outside heat exchange pipe

$\vec{H}^e$ element heat capacity matrix
ΔH enthalpy
k_{hsr} thermal conductivity of MHHSR
$\vec{L}^e$ element load column vector
$\dot{M}$ hydrogen mass absorbed or released
M_{H_2} molecular weight of hydrogen
$\vec{u}_{H_2}$ velocity of hydrogen
$\vec{u}_f$ velocity of heat exchange fluid.
P_f pressure of heat exchange fluid
Q_{ij} weight function
R standard gas constant
$\tilde{s}(x)$ fully smooth S-shaped function
T temperature
T_e represents environmental temperature.
T_f temperature of heat exchange fluid,
τ porosity
ρ_{H_2} density of hydrogen
ρ_{bl} density of metal hydride
ρ_f density of heat exchange fluid
ρ_{hsr} density of MHHSR
μ_f temperature viscosity of heat exchange fluid
$(\rho C_p)_e$ effective volumetric heat capacity
$(\rho C_p)_f$ volumetric heat capacity of heat exchange fluid
λ_e represents effective thermal conductivity
λ_f thermal conductivity of heat exchange fluid
λ_{H_2} thermal conductivity of hydrogen
λ_{bl} thermal conductivity of metal hydrogen bed layer
ϕ_i hydrogen absorption equilibrium pressure polynomial parameter
ξ and γ are local coordination
γ_{hm} ratio of hydrogen to metal atom,
σ_φ Prandtl constant of turbulence energy dissipation rate